

THERMOFORMING SHRINKAGE PREDICTION

SUBMITTED TO POLYMER ENGINEERING & SCIENCE

REVISED 1-FEB-2001

HAIHONG XU AND DAVID O. KAZMER

DEPARTMENT OF MECHANICAL AND INDUSTRIAL ENGINEERING

UNIVERSITY OF MASSACHUSETTS AMHERST

AMHERST, MASSACHUSETTS 01003

Contact: Dr. David O. Kazmer

Engineering Laboratory Building

University of Massachusetts Amherst

Amherst, MA 01003

Fax: 1-413-545-1027

E-mail: kazmer@ecs.umass.edu

ABSTRACT

Most thermoforming product development processes rely on costly and time consuming forming trials to determine adequacy of the mold and process. In this paper, an analytical method is developed for shrinkage predictions on the basis of a visco-elastic constitutive material model with initial conditions from a commercial thermoforming simulation. The theoretical analysis and transfer functions have been developed to accommodate different sets of materials, process conditions, and mold geometry. The shrinkage model consists of a transient thermal analysis for temperature solution; a stretching phase analysis for inflation-induced stress estimation; a post contact analysis for thermal stress and relaxation; and a post-molding strain analysis based on stress solution. The shrinkage prediction analysis has been developed and validated with a complex geometry thermoforming application. The results indicate that the shrinkage estimates provided by the analysis were within the objective tolerances of 0.1%, as measured in terms of absolute prediction error.

KEYWORDS

Thermoforming simulation, thermoviscoelasticity, shrinkage, dimensional tolerancing

1 INTRODUCTION

Thermoforming is a widely used process to manufacture thin-wall polymer parts at relatively low cost. In this process, an exerted pressure differential rapidly deforms the softened polymer sheet to fully contact the mold surface. The formed part is usually held against the mold surface by a pressure differential to facilitate cooling and reduce final shrinkage, after which it becomes capable of sustaining the newly acquired shape. The part is then ejected and trimmed into the final product.

Compared to other polymer conversion processes, little attention has been given to the process control and simulation of thermoforming. Most commercial development processes rely on trial forming, which is costly and time consuming, to decide whether the desired geometry and quality can be attained. Advanced technical applications challenge both the capability of thermoforming processing technology as well as the predictive accuracy of process simulation and dimensional prediction. Additional empirical and analytical work is necessary to support commercial applications with advanced material systems, reduce design and manufacturing cost, and gain tighter process control over the manufacturing process.

In general, the suitability of thin-walled thermoformed parts in tight tolerance applications will be limited by the linear shrinkage of the part relative to required tolerances. While out of plane warpage is significant, thermoformed parts are highly compliant and are easily straightened into the required shape (1,2). However, changes in linear dimension can cause significant strain or buckling during end-use. Thus, the objective of this paper is to estimate the final part dimensions based on evaluation of the residual stresses resulting from the mechanical stretching and cooling of the thermoformed part. First, the material models and theoretical bases of the analysis will be discussed. Then, the approach and detail of analytical process modeling

will be described for evaluation of thermal and stress effects. Third, a summary of empirical work performed to characterize thermoforming shrinkage behavior is documented. Finally, the results of simulations and experiments are compared and evaluated, with a discussion of future improvements.

2 MATERIAL MODELS

2.1 Overview

Prior research has investigated the simulation of the blow molding and thermoforming processes (3-15). Numerical schemes are typically applied to various elastic or visco-elastic constitutive models for large strain stretching simulations. One approach is based on the elastic constitutive model developed by Rivlin (16,17), where the strain energy is assumed to be a function of strain invariants. Another elastic model is developed by Odgen (9,10,18,19), where the strain energy function is given by principal stretches, instead of using strain invariants. Although the Odgen model seems to have more physical meaning by directly utilizing principal stretches, its non-linear parameter terms complicate the experimental fitting significantly. Delorenzi (3) and Nied (14) developed another extensive membrane model to include the non-linear elastic effect for finite element formulation. There is also an approach based on mass conservation and geometry of the mold, developed by Rosenzweig, Narkis, and Tadmor (20), which yields a good approximation to the thickness distribution. These studies show that the thickness distribution is not highly dependent to the material property but more to the geometry of the mold. However, material property and constitutive models may have significant influence over the inflation pressure and time, numerical stability, stress profiles, and thus final solution of shrinkage.

When the polymer sheet is heated above glass transition temperature, it behaves more viscously than a hyper-elastic bubble. The stress relaxation, which occurs during the entire forming process, is also heavily related to the temperature effect. The complexity involved by adding viscosity results in numerous undetermined material coefficients, complicated numerical schemes, and tremendous material characterization requirements. Although the visco-elastic material properties and models do not have the dominant influence over thickness prediction, an efficient material model with viscosity is necessary for evaluating the stress profiles and resulting shrinkage and warpage. Significant research has been devoted to simplify the visco-elastic expression of material behavior. The basic form of the time-strain separable model (21) and the numerical scheme for relaxation evaluation is widely used in FEA simulation of thermoforming process. A more advanced form of time-strain separable model, the Kaye-Bernstein-Kearsley-Zapas model (6,7,18) is becoming more prevalent despite of its complexity in implementation.

The implemented approach utilizes the KBKZ model since numerous materials have been characterized for use with commercial forming simulations. Its use thus reduces the material characterization requirements, and eliminates potential error resulting from use of different constitutive models between the forming and shrinkage simulations. The KBKZ model has a general form

$$\sigma(t) = A(\lambda(t), t) + \int_0^t B(\lambda(t), \lambda(\tau), t - \tau) d\tau \quad (1)$$

For uniaxial stretching, the elongation stress is given

$$\sigma(t) = \int_{-\infty}^t \mu(t-t') \cdot h(I_1 - I_2) \cdot B(t, t') dt' \quad (2)$$

The material memory function

$$\mu(t-t') = \sum_{k=1}^N \left[\frac{a_k}{\tau_k} \exp\left(-\frac{t-t'}{\tau_k}\right) \right] \quad (3)$$

is given by time t , the time variable in relation to t' , and the material dependent parameters a_k , τ_k .

Given the relaxation modulus response over time, $G(t)$, for a reference temperature and small step strain, the corresponding $\mu(t)$ is the derivative of $G(t)$:

$$\mu(t) = G'(t) = \frac{d}{dt} \left[\sum_{i=1}^N \alpha_i \exp(-t/\tau_i) \right] \quad (4)$$

The damping function commonly has one of the following forms (22-24):

$$h(I_1, I_2) = \frac{1}{1 + \alpha \sqrt{(I_1 - 3) \cdot (I_2 - 3)}} \quad (5)$$

$$h(I_1, I_2) = \frac{1}{\exp(\beta \cdot \sqrt{\alpha I_1 + (1 - \alpha) I_2 - 3})} \quad (6)$$

$$h(I_1, I_2) = \frac{\alpha}{(\alpha - 3) + \beta \cdot I_1 + \beta \cdot I_2} \quad (7)$$

which is given by two scalar invariants I_1 , I_2 and the material and temperature dependent parameters α and/or β . The Finger strain tensor $\hat{B}(t, t')$, which is a function of strain rate, is defined as,

$$\hat{B}(t, t') = \begin{bmatrix} \lambda^2(t, t') & 0 & 0 \\ 0 & \lambda^{2m}(t, t') & 0 \\ 0 & 0 & \lambda^{-2(1+m)}(t, t') \end{bmatrix} \quad (8)$$

$$\lambda(t, t') = \exp[\varepsilon_0(t - t')] \quad (9)$$

where $m = -1/2$ for uniaxial elongation, $m = 0$ for planar extension, and $m = 1$ for equibiaxial extension.

Assuming that the temperature dependence follows an Arrhenius relation (25), the stress can be modeled as:

$$\sigma(T) = \sigma(T_0) \exp(-a \cdot (T - T_0)) \quad (10)$$

The Arrhenius parameter, a , is used to define the influence of temperature on material behavior. Another approach to include the temperature effect in the KBKZ model is to use WLF function shifting given by Williams, Landel, and Ferry (WLF) (25,26) equation,

$$\log(a_T) = -\frac{C_1(T - T_0)}{C_2 + (T - T_0)} \quad (11)$$

where C_1 , C_2 are material constants which can be derived from relaxation data, and T_0 is the reference temperature.

2.2 Material characterization

The KBKZ model describes the stress-strain relationship of the polymer under different strain rates. The nonlinearity of the model makes the parameters highly interrelated, less meaningful physically, and hard to determine through experiments separately. The fitting of the KBKZ model is accomplished by comparing the predicted stress-strain relationship with experimental observations. The parameters are derived when the objective of minimizing the prediction error is reached. The material dependent parameters a_k , τ_k , in the material memory function (Equation 3), and the Arrhenius parameter a which gives the temperature effect (Equation 10), can be determined simultaneously if the experimental data on groups of stress-strain curves under different strain rates and temperature are available.

Lubricated compressive experiments (27) have been conducted for a common thermoforming grade of ABS to obtain true stress and strain data under different strain rates and temperature for material model fitting. The ABS specimen (25mm*25mm*7.3mm) is placed

under a compressive testing system (Instron 5566 Material Testing System) after equilibrating at designated temperatures (180C, 185C, and 190C). To create a slip condition and reduce edge effects, silicone oil is applied to the surfaces of the specimens.

Figure 1 and 2 are the fitting results of the observed stress at different strain rates and temperatures. The ABS model parameters are listed in Table 1, and are applied to the analytical shrinkage model for stress evaluation at the end of the stretching stage. The R-square error for the resulting fits was within one percent of the experimental data.

3 ANALYTICAL PROCESS MODELING

3.1 Shrinkage modeling

Shrinkage is the combined effect of structural stress accumulation due to stretching and thermal stress accumulation due to constrained cooling. Thus, the stress accumulation and subsequent relaxation can be used to determine the strain distribution, and finally, the shrinkage, which is the integral of strain along a geometric profile. The KBKZ model is an accurate representation of the stress-strain relationships of polymeric materials, and is capable of defining the nonlinear behavior under different strain rates and temperatures. Because the physical constraint of the material by the mold will convert thermal contraction strain into thermal stress, both the Young's Modulus and the expansivity of the material are important to characterize. The expansivity can be described by the coefficient of thermal expansion or the pressure, volume and temperature curves modeled with a double-domain fit (28). The methodology of analytical shrinkage prediction is drafted in Figure 3.

Figure 3 indicates that the shrinkage analysis consists of: 1) a thermoforming simulation for the solution of the thickness distribution; 2) a transient thermal analysis for temperature solution; 3) a stretching phase analysis for inflation-induced stress estimation; 4) a post contact

analysis for thermal stress and relaxation; and 5) a post-molding strain analysis for shrinkage estimation. A commercial blow molding and thermoforming simulation was utilized to simulate the heating of the sheet, sag, mold closure, pre-inflation, inflation, and the resulting thickness and strain distribution. The detail of the developed shrinkage model formulation, and the procedure for each subsequent analysis stage are discussed next.

3.2 Thermal Analysis

Thermal analysis is used to derive the temperature history at each location of the polymer sheet, which is necessary for estimation of the thermal dependent stress accumulation and relaxation. The thermal analysis is assumed to be independent of the structural loading and this decoupled from the stress analysis.

Polymeric materials are poor heat conductors and thus most heat conductance will occur in the direction normal to the plane of the sheet. As such, the problem can be reduced to a one-dimensional transient thermal analysis. The finite difference method (29,30) is suitable for solving this problem with simple geometry and boundary conditions. The temperature relationship among neighboring nodes at incremental time steps for are:

$$(1 + 2F_0)T_m^{p+1} - F_0(T_{m-1}^{p+1} + T_{m+1}^{p+1}) = T_m^p \quad \{\text{Node internal to sheet}\}$$

$$(1 + 2F_0 + 2F_0B_i)T_0^{p+1} - 2F_0T_1^{p+1} = 2F_0B_iT_\infty + T_0^p \quad \{\text{Node on surface}\} \quad (12)$$

where

$$F_0 = \frac{\alpha \cdot \Delta t}{(\Delta x)^2} \quad (13)$$

$$B_i = \frac{h\Delta x}{k}$$

and h is the heat convection coefficient, Δx is the layer thickness, Δt is the time increments, k is the thermal conductivity, and α is the thermal diffusivity. An implicit numerical method was utilized to provide control of the time step and mesh creation. Gauss-Seidel iteration (31) is used

instead of matrix inversion in order to optimize solution speed. It should be noted that the thermal contact resistance and heat transfer coefficient does vary during the cycle (32), and is dependent upon the process dynamics as well as the material properties of the polymer and mold. A value of 1000 W/mC was selected for h according to these previous findings and found to correlate well with process measurements taken during validation.

3.3 Stress analysis of the stretching phase

The objective of this section is to provide an analytical estimation of the mechanically accumulated stress from an estimated thickness distribution of the thermoformed part. The stretching history is highly dependent on the geometry of the mold, forming pressure, temperature and other factors. A general analytical solution of the stretching history is difficult to derive for complex geometry because of its dependency with location. The entire stretching usually occurs within a fraction of a second, although the duration of the stretching is dependent on the contact location. It is observed in thermoforming trials that the polymer sheet contacts the closest flat surface of the mold first with minimum stretching, while other areas of the sheet continue to stretch into the corners until the part is fully formed. In many thermoforming applications, strong vacuum or pressure assist is used to ensure that the sheet contacts small features of the mold. The large pressure difference between two sides of the sheet purposely drives the sheet stretching much more quickly than inflation under the kinetic equilibrium.

To simplify the analytical solution, the entire polymer sheet is assumed to be expanding at a constant stretch rate until it contacts the mold.

$$\dot{\epsilon} = \text{const} \tag{14}$$

The stress load resulting from the pressure difference on an expanding spherical membrane can be estimated as (31,33),

$$\sigma \approx \frac{PR}{2b} \quad (15)$$

where P is the applied pressure, R is the expanding radius, and b is the membrane thickness. The elastic liquid response of polymer to the applied stress has the form,

$$\sigma = \eta_e \cdot \dot{\varepsilon} \quad (16)$$

where η_e is the apparent viscosity of the polymer flow. Considering the different conditions at the beginning and the end of the stretching, the average stretch rate can be estimated as,

$$\dot{\varepsilon} = \frac{P}{2\eta_e} \left[\frac{R_0}{2b_0} + \frac{R_{cor}}{2b_{cor}} \right] \quad (17)$$

where R_0 represents the estimated radius of the inflated sheet when it initially contact the mold, and R_{cor} represents the radius of the smallest feature of the part and the corresponding thickness after stretching.

The biaxial extension of the polymer sheet coincides with contraction in the thickness direction (27,34). By assuming material incompressibility and homogeneous deformation, the Hencky strain in the thickness direction is given by

$$\varepsilon = \ln(b/b_0) \quad (18)$$

where b is the sheet thickness as a function of time. The strain rate is,

$$\dot{\varepsilon} = \frac{d\varepsilon}{dt} = \dot{b}/b \quad (19)$$

The corresponding biaxial extension under as incompressible assumption becomes,

$$\dot{\varepsilon}_b = -\dot{\varepsilon}/2 = -\frac{1}{2} \dot{b}/b \quad (20)$$

The above reasoning relates the in-plane strain and strain rate directly to the thickness distribution across the polymer sheet resulting from the sheet re-heating, sag, pre-inflation, and

inflation. The final thickness distribution is stable and easy to obtain either experimentally or numerically from available commercial simulations. Employing the measured thickness distribution, the stress and strain distributions at the end of the stretching phase can be estimated using the described models with the described KBKZ constitutive model.

3.4 Stress analysis in the post contact cooling stage

The stretching stops when the polymer sheet fully contacts the mold. As the sheet temperature drops, the part gains stiffness and capability to sustain the shape of the mold. The strain involved in the cooling stage is negligible compared to that in the stretching stage, and is readily estimated using elastic material models. However, the significant temperature drop and the relatively long cooling time span (relative to the characteristic relaxation time of the polymer at processing temperatures) imply that the thermal effect on relaxation and shrinkage behavior cannot be overlooked. The stress accumulation during the cooling stage is mostly thermally induced. After the part is ejected, the residual stress will be released and subsequently cause shrinkage and warpage.

Taking into account the stress relaxation and the variation of Young's Modulus over time, a numerical approach is derived as follows. When the part is constrained by the mold surface, the thermal residual stress increment without relaxation at time t is given by

$$\Delta\sigma(t) = (\alpha - \alpha_{mold}) \cdot [T(t) - T(t + \Delta t)] \cdot E(T(t)) \quad (21)$$

and considers the effect of the mold's thermal expansion. The stress can be evaluated with successive iterations,

$$\sigma(t + \Delta t) = [\sigma(t) + \Delta\sigma(t)] \cdot g(\Delta t, T(t)) \quad (22)$$

where $g(\Delta t, T(t))$ is the relative relaxation modulus at temperature $T(t)$ for time span Δt as characterized by the KBKZ constitutive model. The stress just prior to mechanical release,

$\sigma(t_{release})$, can then be derived using this analysis with the initial conditions provided from the analysis of previous sections.

3.5 Shrinkage analysis

Upon release from the mold, the accumulated residual stress will drive shrinkage in the thermoformed part, followed by additional thermal contraction as the part cools to the end-use temperature. The free shrinkage in the x direction, from position x_1 to position x_2 , ($x_2 > x_1$), can be roughly estimated as

$$S = \left[\alpha(T_g - T_{end}) - \alpha_{mold}(T_{mold} - T_{end}) \right] (x_2 - x_1) + \int_{x_1}^{x_2} \frac{\sigma_{acc}(x)}{E(x)} dx \quad (23)$$

where α and α_{mold} are the thermal expansion coefficient of the polymer and the mold, T_{end} is the end use temperature of the thermoformed part, $\sigma_{acc}(x)$ is the x direction stress component at position x accumulated across the thickness when the sheet fully contacts with mold, and $E(x)$ is the location dependent modulus at the time of part ejection. Under mechanical constraints of the sheet common for male forming or pressure vacuum holding of the parts during the cooling phase, the thermal stress will be accumulated and experience significant relaxation before released as strain. Thus, the first term of equation (23) requires the form of integration over geometry and cannot be simplified as the product of temperature drop and the coefficient of thermal expansion. Another analytical model is proposed below to include the constraint effects in the cooling phase. As such, the corresponding shrinkage is,

$$S = \int_{x_1}^{x_2} \left\{ \alpha [T_{release}(x) - T_{end}] - \alpha_{mold}(T_{mold} - T_{end}) \right\} dx + \int_{x_1}^{x_2} \frac{\sigma(t_{release})}{E(x, T_{release})} dx \quad (24)$$

$T_{release}$ and $t_{release}$ are the temperature and the time when the part is no longer constrained by the mold surface. For male molding, the release happens when the part is ejected. For female

molding, the release happens when the pressure or vacuum holding of the part stops. For parts with complex features, the release can be governed by either or both of the two scenarios. In some case, the holding pressure or vacuum is not sufficient to maintain the contact with the mold surface. The stress threshold which may trigger the release can be estimated as, $\sigma_{release} = P \cdot f_s$, where P is the holding pressure, and f_s is the static friction coefficient.

4 RESULTS AND DISCUSSION

4.1 Experimental

The thermoforming process is a combination of a complex series of events, such as the clamping and removal of the polymer sheet, the shuttling of sheet from station to station, the open and closing of the mold platens, the exertion of pressure and vacuum, the air-assist part ejection, and the on/off of the cooling fans. This sequence of events can be programmed into a sophisticated thermoforming machine with position, temperature, pressure and time control to perform a specific thermoforming task. To retrieve the necessary information on process setting required by future analytical modeling, the forming trials and the capability of thermoforming machine have been closely investigated.

Figure 4 charts several events that occurred during a typical female part forming cycle. The duration of each event is marked by the solid line. The dotted lines demonstrate the movement of the top and bottom platens, where the mold and the pressure box were mounted. The polymer sheet is heated up by the oven, and then shuttled to the forming station at the signal of the machine infrared sensor inside the oven. After the mold is engaged, pressure or vacuum is applied to shape the polymer sheet into the mold with respect to specific forming technique in use. The mold will be completely open and the part ejected at the end of the forming cycle.

The thermoforming machine was extensively instrumented for the purpose of analysis validation. In the machine's process settings, the start time is taken as the time when the position sensors in the forming station are triggered. However, the initial time of the analysis is assumed to be beginning of the stretching phase, which make the model cycle time always less than the actual machine forming cycle time. The initial sheet temperature is assumed to be uniform (profiling not taken into account). In the validation trials, the sheet temperature was measured by infrared sensors located in the oven and forming station. The actual temperature at the forming station was found to be several degrees cooler than the machine setting because of either 1) radiant heat from the oven heaters reflected off the polymer sheet, or 2) subsequent cooling during the sheet shuttling from the oven to the forming station. There could also be through-thickness and cross-sheet temperature gradients that could not be characterized. As such, the initial sheet temperature was assumed to be constant until the point of contact with the mold. It is believed that the temperature drop during this short time is not significant.

The actual pressure on the sheet during forming was also found to vary from the specified machine settings. In fact, the sheet was found to be completely formed before the observed pressure reached its specified maximum. As such, the simulation would be most accurate by utilizing the observed pressure trace from the process sensor. However, this information is never available at the prior to manufacturing trials, so the described analysis utilizes an average pressure to estimate inflation stresses.

As discussed, the shrinkage analysis assumes that there is no relative movement between sheet and mold after contact. Some assumptions are made on the total time from the sheet contact with the mold to it is lost contact with the mold for male and female mold. For male forming, the period is assumed to be identical to in-mold cooling time as observed from the

event chart; for female forming, as pressure holding time as observed from the event chart. Caution needs to be exercised when interpreting shrinkage estimates on predominantly female molds with some male features.

4.2 Thickness results

A commercial thermoforming finite element analysis (FEA) was used to obtain the thickness distribution input for the shrinkage simulation (7). The FEA utilizes the KBKZ model and specializes in simulating the inflation of thermoforming to predict the wall thickness and temperature distributions according to the material properties, process conditions, and geometry of the mold. To have confidence in the thickness distribution from the FEA as input for the shrinkage analysis, validation on male and female geometries were performed. The process conditions of the thermoformed parts were optimized to satisfy their quality requirements as summarized in the event chart of Figure 4 and listed in Table 2.

Figures 5 and 6 shows that the simulation results (smooth lines) are in good agreement with the observed point thickness measurement. The simulation results indicate reduced accuracy in complicated features and plug driving areas. However, FEA is an effective estimator of the thickness distribution for a specific thermoforming application, taking into account its sensitivity to geometry, process and materials. The nodal topology and thickness solution were imported directly into the shrinkage simulation for the shrinkage analysis.

4.3 Shrinkage results

Xu et. al. (35) found that the dimensional repeatability in commercially thermoformed parts, as measured by the standard deviation obtained by physical part measurements, is approximately 0.05% of the nominal dimension. This level of manufacturing consistency

provided a goal for the prediction accuracy of the shrinkage analysis for thermoformed parts, since the shrinkage analysis need not be more accurate than the consistency of the process. Due to potential product variation, shrinkage measurements were taken with a FeroArm location capture device at three different locations and averaged across replicate parts. The observed and predicted shrinkage results for parts thermoformed with the female and male mold at nominal conditions are compared in Tables 3 and 4.

Referring to Figures 5 and 6, the centerline dimension in the longitude direction was denoted as X , and the dimension across the bottom edges of the part are marked as $Y1$ and $Y2$ for the deeper end and shorter end, respectively. Every shrinkage prediction provided by the described analysis was within repeatability of the manufacturing process. Thus, the shrinkage analysis project successfully accomplished its accuracy objective, which was initially selected by the part-to-part variation observed in commercial thermoforming processes (35).

4.4 Discussion

Some discussion of the results is warranted. First, it should be noted that the observed shrinkage for parts thermoformed with the female mold is approximately 0.06% greater than parts thermoformed with the male mold. This result would be expected since the female mold does not physically constrain the part during cooling, allowing the part to pull away from the mold and freely shrink with little stress accumulation. By comparison, parts thermoformed with the male mold are fully constrained, develop significant thermal stresses that may relax, and subsequently encounter lower part shrinkage upon part ejection. The developed shrinkage analysis slightly under-predicted the effect of mold constraints, with an average effect of 0.04%.

It should also be noted that the observed shrinkage rates vary significantly dependent upon location within the thermoformed part. This result would likewise be expected since local

draw ratios impact initial stress distributions, thickness distributions, cooling rates, and ejection temperatures. The described shrinkage analysis reasonably predicted a location dependent variance of 0.025% versus the observed variance of 0.032%. This result is significant since it 1) validates the geometric dependence of the shrinkage prediction, and 2) provides insight into thermoforming part warpage, which is largely caused by non-uniform shrinkage across the thermoformed part. As previously introduced, bending effects are not included in the analysis model, which may bring considerable deviation to shrinkage measurements in certain cases. The bending and warpage is difficult to evaluate in finite element analysis because of the complexity in boundary conditions, thermal effects, and material models. Moreover, out of plane compliance of the part may allow the part to be easily deformed to fit the end-use application. Thus, the out of plane deformation should be further characterized with industry observations.

Finally, it should be noted that issues of observability and controllability are prevalent in tight tolerance thermoforming. Specifically, the described shrinkage analysis is a predictive tool which requires the estimation of process parameters that have not yet been observed. As such, significant variances from prediction may be encountered in the product development due to inadequacy of assumptions regarding the process pre-inflation, timings, temperatures, or pressures. Moreover, the ability to control and adjust multiple dimensions simultaneously has not been addressed. Thus, tight tolerance thermoforming is not yet as well established a practice as tight tolerance injection molding, wherein tolerances have been commercially realized that are one or more magnitudes tighter than in thermoforming.

5 CONCLUSION

A shrinkage prediction methodology has been developed that implements a KBKZ constitutive model with thermal analysis to evaluate stress accumulation and relaxation in the

thermoforming process. The mold geometry, material properties, process settings, and corresponding boundary conditions were determined for input to a commercial thermoforming simulation and, subsequently, the described shrinkage analysis. The developed analysis proved to be sufficiently accurate to evaluate the final shrinkage of the thermoformed part from its material properties, the forming process settings, and its thickness distribution.

The developed shrinkage analysis provides a functional guide to the tooling and design of thermoforming parts for thermoformers. This analysis is helpful to the product development process, because the thickness is a relatively stable and undemanding feature to characterize experimentally compared to stress, strain, and shrinkage of the part. Moreover, the thickness distribution can be obtained through several commercial FEA packages, which may enable the shrinkage estimation process prior to the production of tooling. The methodology is also capable of estimating the shrinkage based on the strain or the stress components of the bi-axial extension, and can be implemented within commercial FEA packages as a post-analysis add-on shrinkage solver.

BIBLIOGRAPHY

1. S. C. Liu, S. J. Hu, and T. C. Woo, *Transactions of the ASME Journal of Mechanical Design* **118**, 62-67 (1996).
2. A. K. Fathailall and J. R. Dixon, *American Society of Mechanical Engineers, Design Engineering Division (Publication) DE*: Minneapolis, Mn, USA, 1994; pp 9-17.
3. H. G. deLorenzi and H. F. Nied, *Finite Element Simulation of Thermoforming and Blow Molding*; Hanser Publishers: New York, 1991.
4. T. Doll and K. Kouba, *Kunsts Plast Eur*, 17-18 (1996).
5. K. Kouba, O. Bartos, and J. Vlachopoulos, *Polym. Eng. Sci.* **32**, 699 (1992).
6. K. Kouba, M. O. Ghafur, J. Vlachopoulos, and W. P. Haessly, *Annual Technical Conference - ANTEC, Conference Proceedings*: San Francisco, Ca, USA, 1994; pp 850-853.
7. K. Kouba and P. Novotny, *Thermoforming Quarterly*, 1998; Vol. Fall, p 13.
8. K. Kouba, *TSIM*, C. 1; 3.3 ed., 1994-1998.
9. B. L. Koziey, J. Pocher, J. J. Tian, and J. Vlachopoulos, *Annual Technical Conference - ANTEC, Conference Proceedings*: Toronto, Can, 1997; pp 714-719.
10. B. L. Koziey, M. O. Ghafur, J. Vlachopoulos, and F. A. Mirza, *Composite Sheet Forming*; Bhattacharyya, D., Science, E., Eds., 1997.
11. D. Laroche and F. Erchiqui, *J Reinf Plast Compos*, 230-239 (2000).
12. D. Laroche, K. K. Kabanemi, L. Pecora, and R. W. Diraddo, *Polym Eng Sci*, 1223-1233 (1999).
13. P. D. Luca, A. K. Pickett, and A. F. Johnson, *Mechanical Engineering*, 98-100 (1996).

14. Nied, H. F., Taylor, C. A., and deLorenzi, H. G., *Polym Eng Sci* **30**, 1314-1322 (1990).
15. C. A. Taylor, H. G. DeLorenzi, and D. O. Kazmer, *Polym Eng Sci* **32**, 1163-1173 (1992).
16. R. S. Rivlin, *Philos. Trans. Royal Soc.* **A240**, 459-490 (1948).
17. R. S. Rivlin, *Philos. Trans. Royal Soc.* **243**, 251-288 (1951).
18. R. I. Tanner, *Engineering rheology*; 2nd ed.; Oxford University Press: Oxford ; New York, 2000.
19. R. W. Odgen, *Proceedings of the Royal Society, Series A* **326**, 565 (1972).
20. N. Rosenzweig, M. Narkis, and Z. Tadmor, Z., *Polym Eng Sci* **19** (1979).
21. S. R. Hummel, *Mechanical Engineering*; Lehigh University, 1998.
22. M. H. Wagner and A. Demarmels, *J. of Rheol.* **34**, 943 (1990).
23. M. K. Warby and J. R. Whiteman, *Computer Methods in Applied Mechanics and Engineering* **68**, 33-54 (1988).
24. A. C. Papanastasiou, L. F. Scriven, and C. W. Macosko, *Journal of Rheology* **27**, 387-410 (1983).
25. J. D. Ferry, *Visoelastic Properties of Polymers*; 2nd ed.; John Wiley & Sons: New York, NY, 1970.
26. M. L. Williams, R. F. Landel, and J. D. Ferry, *Journal of the American Chemical Society* **77**, 3701 (1955).
27. C. W. Macosko, *Rheology : Principles, Measurements, and Applications*; VCH: New York, NY, 1994.

28. R. Y. Chang, C. H. Chen, and K. S. Su, *Polym Eng Sci*, 1789-1795 (1996).
29. D. Kincaid and W. Cheney, *Numerical Analysis, Mathematics of Scientific Computing*; 2nd ed., 1996.
30. F. P. Incropera and D. P. DeWitt, *Fundamentals of Heat and Mass Transfer*; 4 ed., 1996.
31. S. I. Krishnamachari, *Applied Stress Analysis of Plastics, A Mechanical Engineering Approach*; Von Nostrand Reinhold: New York, NY, 1993.
32. C. J. Yu and J. E. Sunderland, *Polym Eng Sci* **32**, 191 (1992).
33. J. L. Throne, *Polym.-Plast. Technol. Eng.* **30**, 685-700 (1991).
34. S. Chatraei, C. W. Macosko, and H. H. Winter, *Journal of Rheology* **25**, 433-443 (1981).
35. H. Xu, J. Wysocki, D. O. Kazmer, P. Bristow, B. Landa, J. Riello, C. Messina, and R. Marrey, *SPE Thermoforming Quarterly* **13**, 8-16 (2000).

LIST OF TABLES

Table 1: KBKZ parameters for ABS

Table 2: Thermoforming process conditions

Table 3: Comparison of observed and predicted shrinkage for female mold

Table 4: Comparison of observed and predicted shrinkage for male mold

LIST OF FIGURES

Figure 1: KBKZ fitting of ABS at different strain rates

Figure 2: KBKZ fitting of ABS at different temperatures

Figure 3: Analysis methodology for shrinkage prediction

Figure 4: Event chart for thermoforming of a female part

Figure 5: Validation of thickness prediction for male mold

Figure 6: Validation of thickness prediction for female mold

Table 1: KBKZ parameters for ABS

Alpha	Tau (s)
0.626071	175923.95
27.64236	21528.22
500	8918.05

Arrhenius (1/C)	Ref Temp (C)
0.023004679	180

Damping alpha	Damping beta
1	-0.160499666

Table 2: Thermoforming process conditions

Cooling Time (sec)	Cycle time Preset	Holding time	Eject time
Female	120	102	114
Male	120	102	114

Sheet Temp (C)	Oven Preset	Forming Station Infrared	Mold Temp (C)	Coolant Preset	Bottom Surface Thermocouple
Female	171	160	Female	85	85
Male	163	152	Male	83	83

Pressure (KPa)	Vacuum Gage Preset	Vacuum Observed in Mold	Pressure Form Gage Preset	Pressure Observed in Pressure Box
Female	70	70 at 3 sec, starting 2 sec before mold seal	210	210 at 7 sec, starting on mold seal
Male	70	70 at 3 sec, starting 2 sec before mold seal	210	210 at 7 sec, starting on mold seal

Table 3: Comparison of observed and predicted shrinkage for female mold

	Dimension					
	X=1494.41		Y1=627.23		Y2=654.99	
Shrinkage	Observed	Predicted	Observed	Predicted	Observed	Predicted
(mm)	7.24	7.38	3.26	3.35	3.01	3.42
(Rate)	0.48%	0.49%	0.52%	0.53%	0.46%	0.49%

Table 4: Comparison of observed and predicted shrinkage for male mold

	Dimension					
	X=1531.57		Y1=645.44		Y2=658.62	
Shrinkage	Observed	Predicted	Observed	Predicted	Observed	Predicted
(mm)	6.32	6.73	2.67	3.18	2.84	3.19
(Rate)	0.41%	0.44%	0.41%	0.47%	0.43%	0.49%

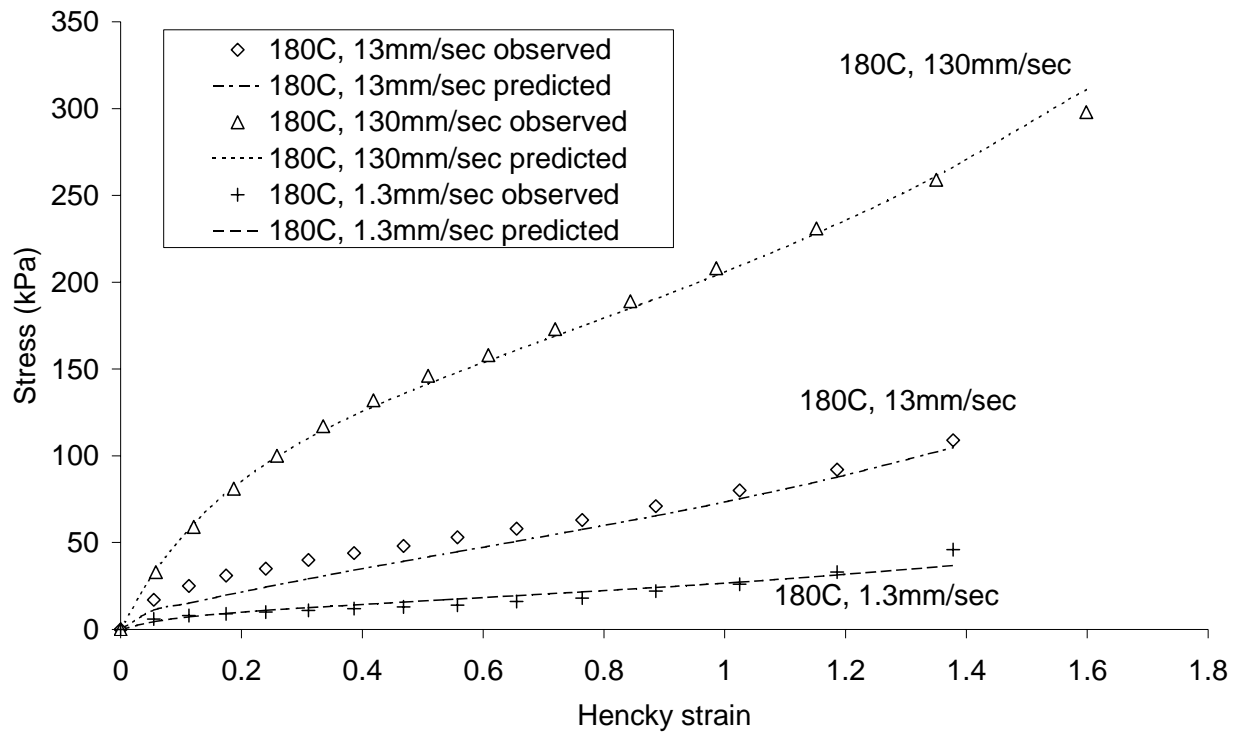


Figure 1: KBKZ fitting of ABS at different strain rates

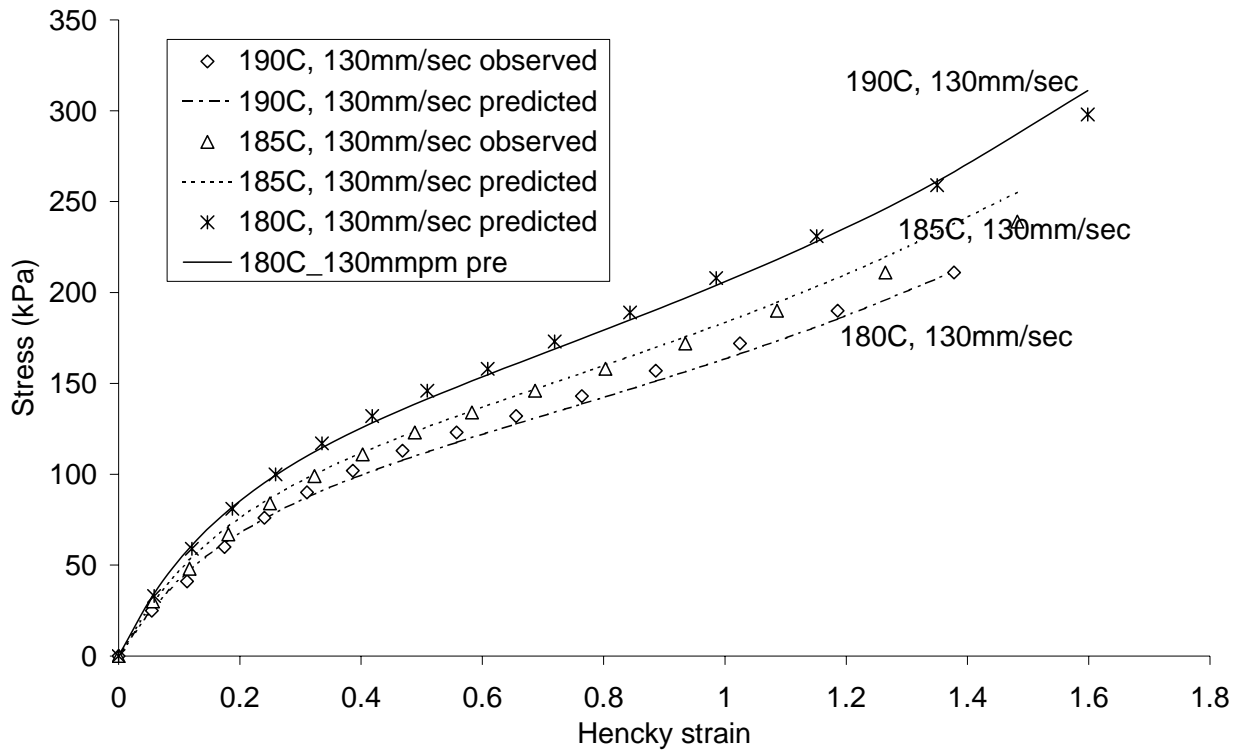


Figure 2: KBKZ fitting of ABS at different temperatures

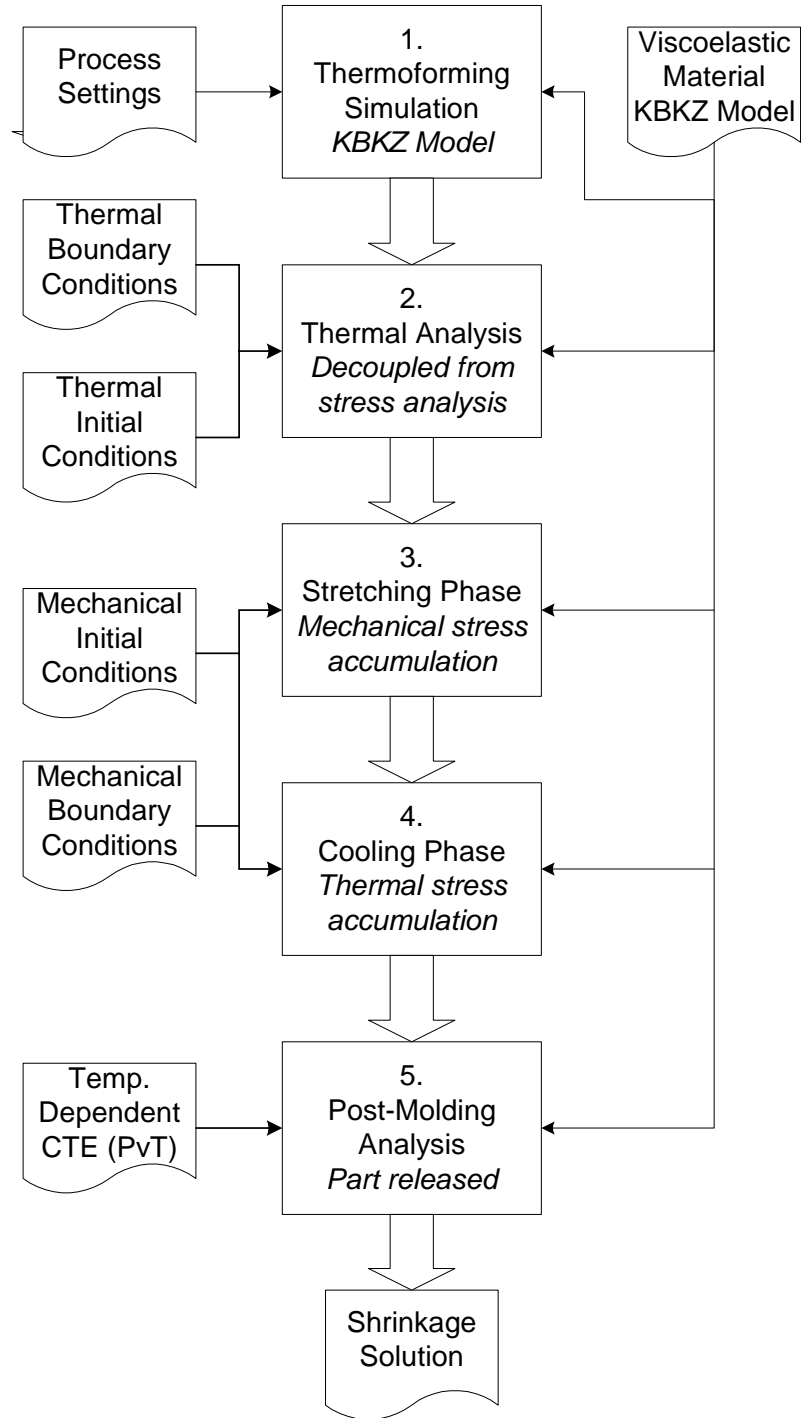


Figure 3: Analysis methodology for shrinkage prediction

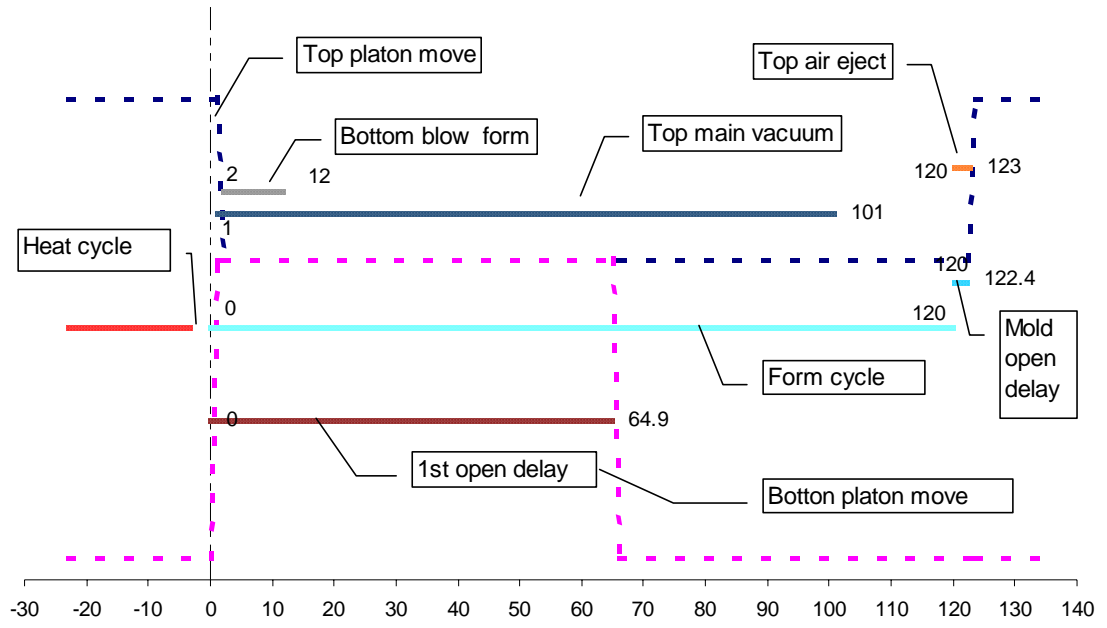


Figure 4: Event chart for thermoforming of a female part

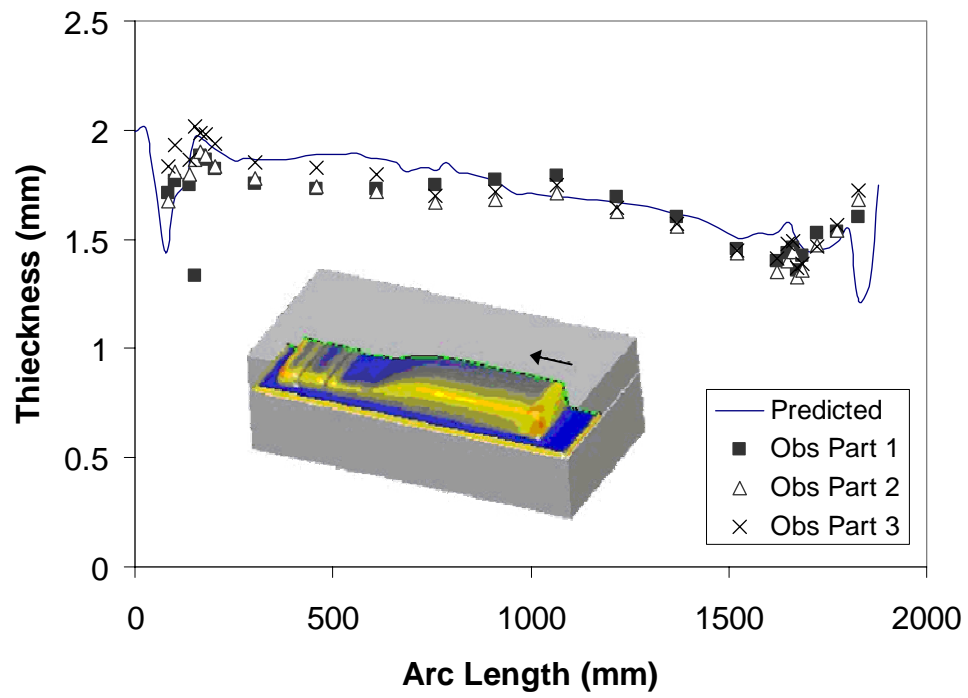


Figure 5: Validation of thickness prediction for male mold

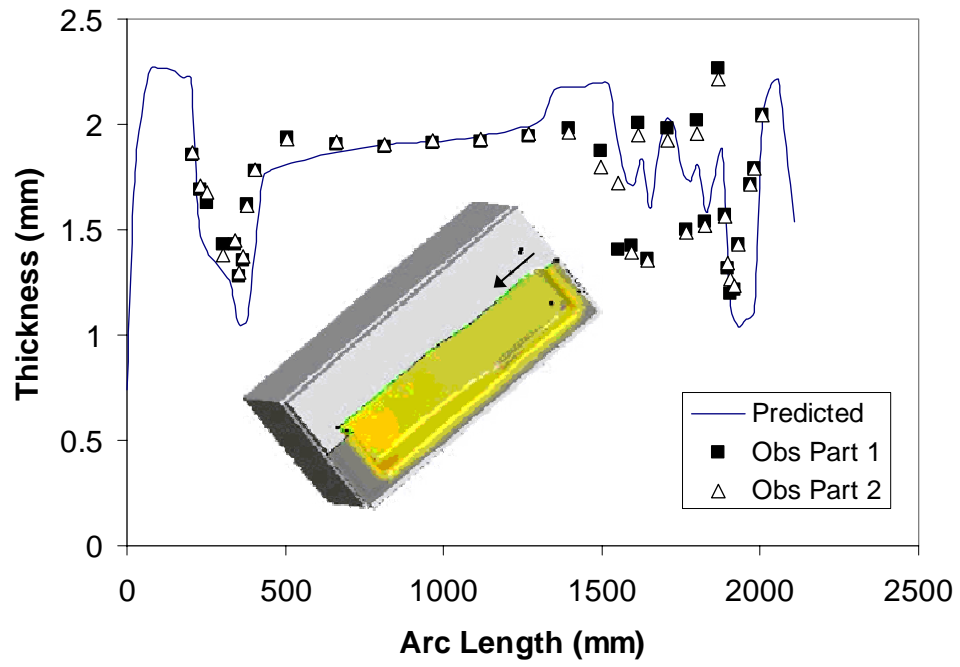


Figure 6: Validation of thickness prediction for female mold